



# Understanding the role of Mg-doped on core-shell structured layered oxide $\text{LiNi}_{0.6}\text{Co}_{0.2}\text{Mn}_{0.2}\text{O}_2$

Ningshuang Zhang <sup>a, b</sup>, Ling Ai <sup>a</sup>, Liping Mao <sup>a, b</sup>, Yaohua Feng <sup>a</sup>, Yingchun Xie <sup>a</sup>, Shengxian Wang <sup>a, b</sup>, Youwei Liang <sup>a, b</sup>, Xiaoling Cui <sup>a, b</sup>, Shiyou Li <sup>a, b, c, \*</sup>

<sup>a</sup> College of Petrochemical Technology, Lanzhou University of Technology, Lanzhou, 730050, PR China

<sup>b</sup> Gansu Engineering Laboratory of Cathode Material for Lithium-ion Battery, Lanzhou, 730050, PR China

<sup>c</sup> Qinghai Research Center of Low-temperature Lithium China -ion Battery Technology, Engineering, Qinghai Green Grass New Energy Technology Co. Ltd., Xining, 810000, PR China



## ARTICLE INFO

### Article history:

Received 15 April 2019

Received in revised form

3 July 2019

Accepted 11 July 2019

Available online 11 July 2019

## ABSTRACT

Mg-doped on core-shell structured layered oxide  $\text{LiNi}_{0.6}\text{Co}_{0.2}\text{Mn}_{0.2}\text{O}_2$  cathodes are synthesized by doping Mg into  $\text{LiNi}_{0.8}\text{Co}_{0.1}\text{Mn}_{0.1}\text{O}_2$  core and  $\text{LiNi}_{0.2}\text{Co}_{0.4}\text{Mn}_{0.4}\text{O}_2$  shell, respectively or Mg co-doped both in core and shell. The influence of Mg doping on crystal structure are characterized by XRD, EDS, XPS and ICP-ES. Electrochemical tests show that doping Mg in the shell layer of  $\text{Li}[(\text{Ni}_{0.8}\text{Co}_{0.1}\text{Mn}_{0.1})_{2/3}(\text{Ni}_{0.2}\text{C}_{0.4}\text{Mn}_{0.4})_{1/3}]\text{O}_2$  (S-Mg) exhibits the optimized electrochemical performance, with retention of 85.79% after 100 cycles at 0.2 C and a high discharge capacity of  $128.4 \text{ mAh g}^{-1}$  at 5 C, compared with C-S, C-Mg, and F-Mg cathodes. Mg-doped in shell layer of Ni-rich cathode material  $\text{LiNi}_{0.6}\text{Mn}_{0.2}\text{Co}_{0.2}\text{O}_2$  can not only maintains the stability of material surface, but also reduces the material impedance. The expansion space of the crystalline host lattice caused by Mg doping in the shell will also promote the transport of  $\text{Li}^+$  during charging and discharging. Cation doping in shell is conductive to electrochemical performance of core-shell materials.

© 2019 Elsevier Ltd. All rights reserved.

## 1. Introduction

In the lithium-ion batteries (LIBs) industry chain, the cost of cathode materials consists more than 30%. Moreover, cathode materials become the key to determine the electrochemical performances of LIBs, especially in energy density and cycling lifetime [1].

In recent years, the Ni-rich cathode materials  $\text{LiNi}_x\text{Mn}_y\text{Co}_z\text{O}_2$  ( $\text{NMC}$ ,  $x \geq 0.6$ ) have attracted wide attention because of its high capacity, good structural stability and low cost compared to commercial  $\text{LiCoO}_2$  and spinel  $\text{LiMn}_2\text{O}_4$  [2,3]. Unfortunately, the Ni-rich  $\text{LiNi}_{0.6}\text{Co}_{0.2}\text{Mn}_{0.2}\text{O}_2$  suffered from the following shortcomings due to the high nickel content of on the surface: 1) Because of the similar size of  $\text{Ni}^{2+}$  (0.69 Å) and  $\text{Li}^+$  (0.76 Å) ions, the  $\text{Li}^+/\text{Ni}^{2+}$  cation mixing occurred so easily that the phase transition irreversibly takes place from layered ( $R3m$ ) to spinel ( $Fd3m$ ) to rock-salt ( $Fm3m$ ) which will ultimately block  $\text{Li}^+$  diffusion [4,5]. 2) The

residual Li formed during the synthesis, appearing as  $\text{LiOH}$  and  $\text{Li}_2\text{CO}_3$  on the surface of Ni-rich materials, would bring about electrolytes decomposition and gas produce. These side reactions can accelerate capacity degradation of batteries [6,7]. 3) During the charging process,  $\text{Ni}^{4+}$  formed in the cathode material has strong oxidation and is reduced spontaneously to  $\text{Ni}^{2+}$  or  $\text{Ni}^{3+}$ . To balance charge, the material releases oxygen, further causing deteriorated thermal stability [8].

Many modification methods have been applied to enhance the structural and chemical stability of Ni-rich cathode such as bulk doping, surface coating, and special structure precursor [9–13]. The core–shell structure has been considered as more effective method to solve the above problems for these layered materials. Because the inner core is mainly composed of high nickel ternary materials that provides high capacity. While outer layer is mainly composed of manganese-rich ternary materials that improves the stability of materials [14,15]. However, although the material of the core-shell structure can improve the shortcomings of  $\text{LiNi}_{0.6}\text{Co}_{0.2}\text{Mn}_{0.2}\text{O}_2$  materials on a certain extent, it also has some drawbacks. Owing to the different composition of core and shell, the core and the shell will separate and produce a void layer during long cycles charge/

\* Corresponding author. College of Petrochemical Technology Lanzhou University of Technology, 36 Pengjiaping Road, Lanzhou, Gansu province, China.

E-mail address: [sylilw@163.com](mailto:sylilw@163.com) (S. Li).

discharge in core-shell materials [16–18].

Doping of ions is considered as an available way to suppress the separation that occurs between two chemically distinct regions and improve the electrochemical performance of core-shell structural materials. Un-Hyuck Kim [19] studied the effect of  $\text{PO}_4^{3-}$  doping the core-concentration gradient-shelled  $\text{Li}_{1.2}(\text{Ni}_{0.133}\text{Co}_{0.133}\text{Mn}_{0.534})\text{O}_2$ . The research showed that the formation of stable Mn-rich and  $\text{PO}_4^{3-}$ -rich shells, was beneficial to alleviate the reaction between  $\text{Ni}^{4+}/\text{Co}^{4+}$  and the electrolyte in the delithiation state and inhibit the aggregation between the primary particles. Seung-Taek Myung [20] investigated compositionally graded Al doping  $\text{Li}(\text{Ni}_{0.76}\text{Co}_{0.09}\text{Mn}_{0.15})\text{O}_2$  material illustrating that the doping Al effectively inhibited micro cracking and maintained the stability of the material structure. In particular, compared with other cations, the doping of Mg ions can more effectively improve the electrochemical performance of layered oxide materials [21,22]. On one hand, the length of a Mg–O bond (0.205 nm) is larger than that of a Ni–O bond (0.1893 nm) which can facilitate the diffusion of  $\text{Li}^+$  ions [23,24]. On the other hand, highly electrochemically reactive and unstable Ni can be partly replaced by inactive Mg reducing the side reactions between the electrolyte and the highly reactive  $\text{Ni}^{4+}$  when charging to high voltage [21].

In order to better understand the role of Mg ions in the core and shell of the core-shell  $\text{LiNi}_{0.6}\text{Co}_{0.2}\text{Mn}_{0.2}\text{O}_2$  material, we firstly prepared the core-doped Mg, shell-doped Mg, and core-shell co-doped Mg of  $\text{LiNi}_{0.6}\text{Co}_{0.2}\text{Mn}_{0.2}\text{O}_2$  materials. Then, we investigated the effect of Mg doping on the electrochemical performances of core-shell materials.

## 2. Experimental

### 2.1. Preparation of cathode materials

A carbonate co-precipitation method was applied for the synthesis of materials. The core-shell of  $\text{LiNi}_{0.6}\text{Co}_{0.2}\text{Mn}_{0.2}\text{O}_2$  material was named as C–S. The core-doped, core-shell co-doped, shell doped Mg of  $\text{LiNi}_{0.6}\text{Co}_{0.2-x}\text{Mn}_{0.2-x}\text{Mg}_x\text{O}_2$  ( $x = 0.02$ ) material was named as C–Mg, F–Mg and S–Mg, respectively. Different molar ratio of Ni/Co/Mn/Mg from  $\text{Ni}(\text{CH}_3\text{COO})_2 \cdot 4\text{H}_2\text{O}$ ,  $\text{Co}(\text{CH}_3\text{COO})_2 \cdot 4\text{H}_2\text{O}$ ,  $\text{Mn}(\text{CH}_3\text{COO})_2 \cdot 4\text{H}_2\text{O}$  and  $\text{MgCl}_2 \cdot 6\text{H}_2\text{O}$  were dissolved in deionized water (0.5 M) to constitute core solution labeled as solution A and shell solution labeled as solution B. The proportions of Ni: Co: Mn: Mg in solution A and B can be referred as Table 1. Among them, the molecular formula of different Mg doping samples is as follows :  $\text{Li}(\text{Ni}_{0.8}\text{Co}_{0.1}\text{Mn}_{0.1})_{2/3}(\text{Ni}_{0.2}\text{Co}_{0.4}\text{Mn}_{0.4})_{1/3}\text{O}_2$  (C–S),  $\text{Li}(\text{Ni}_{0.8}\text{Co}_{0.085}\text{Mn}_{0.085}\text{Mg}_{0.03})_{2/3}(\text{Ni}_{0.2}\text{Co}_{0.4}\text{Mn}_{0.4})_{1/3}\text{O}_2$  (C–Mg),  $\text{Li}(\text{Ni}_{0.8}\text{Co}_{0.09}\text{Mn}_{0.09}\text{Mg}_{0.02})_{2/3}(\text{Ni}_{0.2}\text{Co}_{0.39}\text{Mn}_{0.39}\text{Mg}_{0.02})_{1/3}\text{O}_2$  (F–Mg),  $\text{Li}(\text{Ni}_{0.8}\text{Co}_{0.1}\text{Mn}_{0.1})_{2/3}(\text{Ni}_{0.2}\text{Co}_{0.37}\text{Mn}_{0.37}\text{Mg}_{0.06})_{1/3}\text{O}_2$  (S–Mg).

In addition, 0.5 M  $\text{Na}_2\text{CO}_3$  was labeled as solution C. The solution A was pumped into a continuously stirred reactor with a certain flow rate. At the same time, the solution C was also pumped into a continuously stirred reactor with a certain flow rate. The pH of the solution in the reactor was controlled between 8.0 and 9.0 by controlling the rate of liquid addition of solution A and solution C.

**Table 1**

The different molar ratios of core solutions and shell solutions in C–S, C–Mg, F–Mg and S–Mg samples.

	Solution A				Solution B			
	Ni/mol	Co/mol	Mn/mol	Mg/mol	Ni/mol	Co/mol	Mn/mol	Mg/mol
C–S	0.5333	0.0666	0.0666	0.0000	0.0666	0.1333	0.1333	0.0000
C–Mg	0.5333	0.0566	0.0566	0.0200	0.0666	0.1333	0.1333	0.0000
F–Mg	0.5333	0.0600	0.0600	0.0133	0.0666	0.1300	0.1300	0.0066
S–Mg	0.5333	0.0666	0.0666	0.0000	0.0666	0.1233	0.1233	0.0200

Also, the reactor maintained the reaction solution at a constant temperature of 75 °C and with stirring speed of 600 r min<sup>-1</sup>. When the metal ions in solution A were completely precipitated, solution B was pumped into a continuously stirred reactor with a same certain flow rate. Simultaneously, solution C was added at the same rate to keep the temperature and pH constant in the reactor. The as-prepared precursor was filtered, washed, and dried at 100 °C for 12 h. Then the precursors were preheated at 450 °C for 5 h °C and were mixed with  $\text{CH}_3\text{COOLi}$  in a ratio of 1: 1.08. Finally, the core-shell and Mg-doped  $\text{LiNi}_{0.6}\text{Co}_{0.2}\text{Mn}_{0.2}\text{O}_2$  materials were synthesized by sintering at 850 °C for 12 h under  $\text{O}_2$  atmosphere. Fig. 1 is the schematic illustration of Mg doping core-shell  $\text{LiNi}_{0.6}\text{Co}_{0.2}\text{Mn}_{0.2}\text{O}_2$  particle.

### 2.2. Materials characterization

The XRD patterns were represented by powder X-ray diffraction with  $\text{Cu K}\alpha$  radiation and the diffraction angle  $2\theta$  range of 10°–70°.

The morphology and element distribution in cross section of materials were examined by scanning electron microscopy (SEM, JSM-5600, Japan) and Energy dispersive X-ray spectroscopy (EDS).

The  $\text{Ni}_{2p}$ ,  $\text{C}_{1s}$ , and  $\text{Mg}_{1s}$  binding energies of the particles surface were measured by XPS (GG 314-JPS-9200) techniques.

ICP-AES was employed to measure the electrodes which were charged to 4.3 V and then put in electrolyte at vacuum dryer under 328 K for two weeks. The number of transition metal (Ni, Co, and Mn) which dissolved in electrolyte was gauged through ICP-AES.

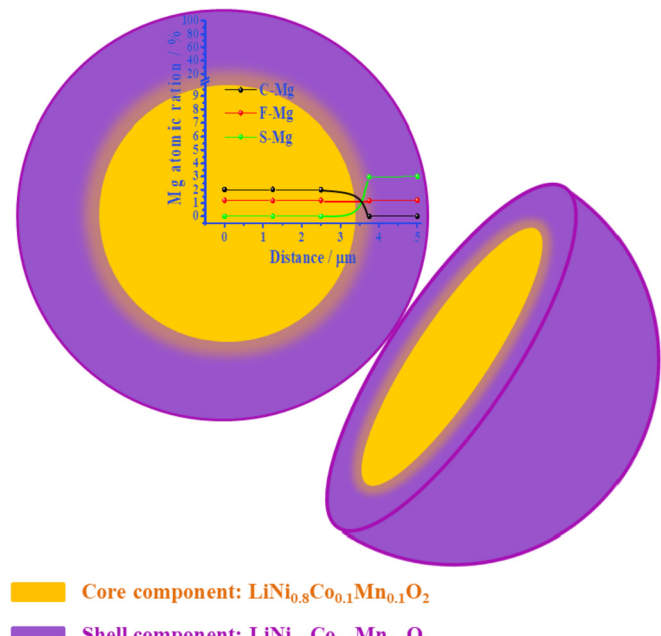


**Fig. 1.** Schematic illustration of core-shell structure with Mg-doped  $\text{LiNi}_{0.6}\text{Co}_{0.2}\text{Mn}_{0.2}\text{O}_2$ .

### 2.3. Electrochemical characterization

The active material powders, polyvinylidene fluoride (PVDF), and acetylene black were mixed with a weight ratio of 8:1:1 in N-methyl-pyrrolidone. The loading of the active material on the aluminum foil is  $1.14 \text{ mg cm}^{-2}$ . The slurry was coated on an Al foil and dried at about  $120^\circ\text{C}$  for 12 h. The 2032 coin-type cells were assembled in an argon atmosphere glove box using lithium metal as negative electrode, the prepared electrode material as cathode, and  $1 \text{ mol L}^{-1}$  LiPF<sub>6</sub>-ethylene carbonate (EC)/diethyl carbonate(DEC) (1:1,v/v) as the electrolyte.

The charge and discharge tests was performed on a LAND CT2001A tester (Wuhan, China) from 3.0 V to 4.3 V at  $25^\circ\text{C}$ .

The electrochemical impedance spectroscopy (EIS) analysis on CHI660C electrochemical analyzer with three-electrode system (Shanghai, China) was measured at the fully delithiated state of 4.3 V between 100 kHz and 10 mHz with 5 mV amplitude.

### 3. Result and discussions

XRD patterns of the C-S, C-Mg, F-Mg and S-Mg materials are shown in Fig. 2 All the XRD patterns have no impurity peaks and fit well with hexagonal  $\alpha\text{-NaFeO}_2$  structure belonging to the R-3m space group. The obvious splitting of (006)/(102) and (108)/(110) peaks in all XRD patterns indicates the formation of a well-ordered layered structure for all samples [25]. The result suggests that the layer structure isn't destroyed by the substance of Mg. For the sake of understanding the influence of Mg doping on the crystal structure of materials, the lattice parameters are calculated on Table 2. It can be observed that the values of lattice parameters c gradually increase with the doping Mg. Due to the radius of the Mg ion is larger than the radius of the Co and Mn ions, which will enlarge the space of crystal lattice when the Mg ions have entered the lattice and partly replace Co and Mn ions. The increase in c-lattice parameter is beneficial for the transfer of Li [22,26,27]. In general, a higher ratio of the lattice constant c/a of S-Mg indicates its better layered structure [28]. Moreover, the ratio of I (003)/I (104) can reflect the degree of Li<sup>+</sup>/Ni<sup>2+</sup> cation mixing. The larger I (003)/I (104) value indicates a lower cation mixing [29]. Compared with the C-S, C-Mg, and F-Mg sample, the ratios of I (003)/I (104) in S-Mg materials significantly are bigger. This indicates that the doping Mg in the surface layer of the core-shell structure can effectively reduce the degree of cation mixing of the material and

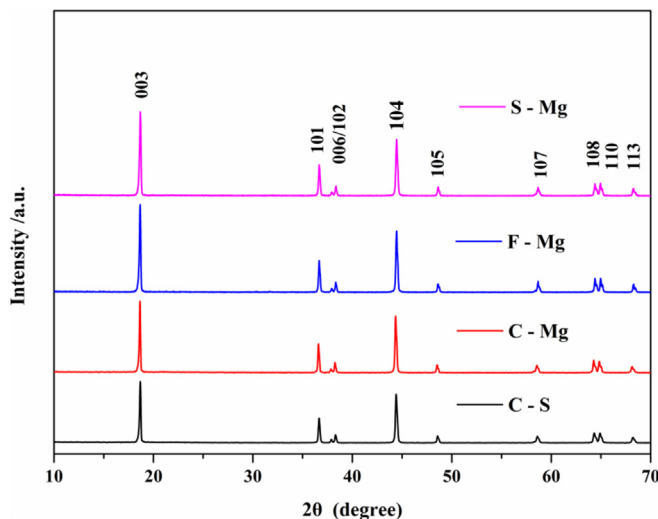


Fig. 2. XRD patterns of C-S, C-Mg, F-Mg and S-Mg powders.

**Table 2**  
Lattice parameters of C-S, C-Mg, F-Mg and S-Mg samples.

Sample	a (Å)	c (Å)	c/a	$I_{003}/I_{104}$
C-S	2.8747	14.2301	4.9502	1.2630
C-Mg	2.8737	14.2305	4.9519	1.2648
F-Mg	2.8717	14.2307	4.9554	1.4310
S-Mg	2.8715	14.2312	4.9560	1.4867

accelerate the transmission of Li ions [30]. Hence, it can be expected that S-Mg materials have better electrochemical performance.

To prove that the designed distribution of each metallic element is realized, the morphologies and the elemental distribution on the cross-section of the C-S, C-Mg, F-Mg and S-Mg materials are studied by SEM and EDS in Fig. 3. As shown in Fig. 3 (a, b, c, d), all the powders exhibit spherical shape with an average particle size of 10 μm. There are no distinct differences of particle morphology or size by Mg ions doping. Fig. 3(e) displays that the design of core-shell sample is: the core is composed of  $\text{LiNi}_{0.8}\text{Co}_{0.1}\text{Mn}_{0.1}\text{O}_2$  and the shell is composed of  $\text{LiNi}_{0.6}\text{Co}_{0.4}\text{Mn}_{0.4}\text{O}_2$ , which is an average composition of  $\text{LiNi}_{0.6}\text{Co}_{0.2}\text{Mn}_{0.2}\text{O}_2$ . Therefore, the content in Ni significantly decreases while that of Co and Mn increases from core to the shell of the particle [31,32]. Fig. 3(f) clearly demonstrates that the Mg ions are uniformly doped in the core of the material, and Mg ions are not detected in the shell of the material. However, the constant concentration of Mg ions is uniformly distributed throughout the particle in Fig. 3(g). Fig. 3(h) clearly verifies that the content of Mg is not detected in the core portion of the material and the Mg ions are successfully doped into the shell of the material [33].

XPS measurement was used to study further assisted proofs for the decreased degree of Li<sup>+</sup>/Ni<sup>2+</sup> cation mixing and the amount of  $\text{Li}_2\text{CO}_3$  after Mg doping. The valence states of Ni, C, Mg on the surface of C-S, C-Mg, F-Mg and S-Mg materials are investigated. According to the matching XPS data, the consequence of XPS spectra Ni 2p<sub>3/2</sub> demonstrates that Nickel exists as both Ni<sup>2+</sup> and Ni<sup>3+</sup> in all of the materials [34]. As shown in Fig. 4(a, d, g, j) it can be observed that the Ni 2p<sub>3/2</sub> peaks of C-S and C-Mg material locates

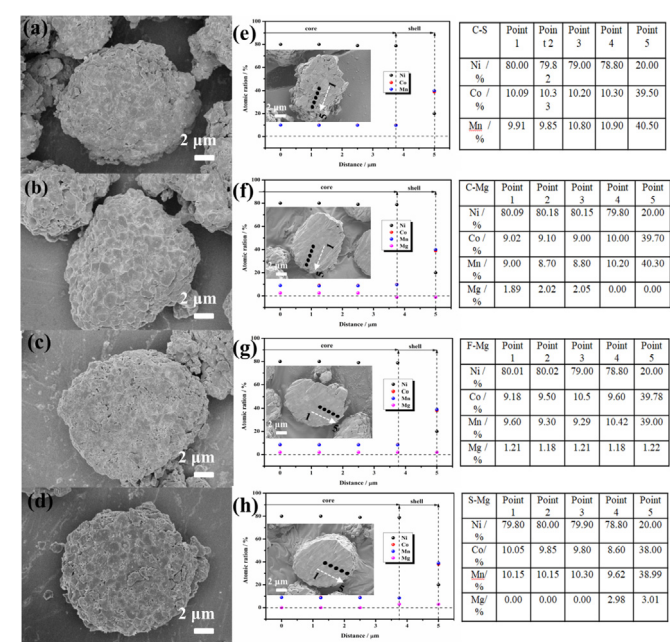
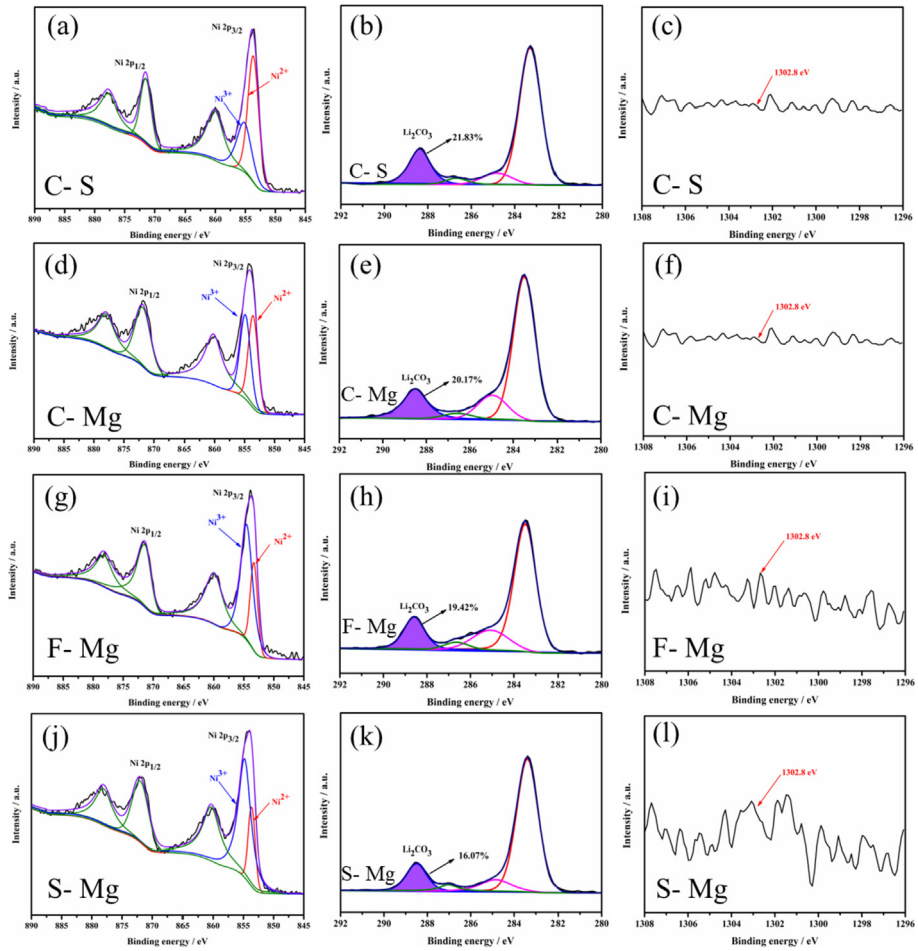


Fig. 3. SEM and EDS images of the C-S (a, e), C-Mg (b, f), F-Mg (c, g) and S-Mg(d, h).



**Fig. 4.** XPS spectra and fitting results of C-S, C-Mg, F-Mg and S-Mg samples: (a)(d)(g) (j) Ni 2p, (b)(e) (h)(k) C 1s, (c)(f) (i)(l) Mg 1s.

at 853.58 eV and 853.78 eV. Whereas, the Ni 2p<sub>3/2</sub> peaks of F-Mg and S-Mg are observed at 853.98 eV and 854.28 eV, respectively. This phenomenon indicates that less Ni<sup>2+</sup> exists on the surface of S-Mg material in comparison with C-S, C-Mg and F-Mg. This result demonstrates that the doping Mg in the shell layer of the core-shell structure has lower degree of cation mixing, which is also consistent with the result in Fig. 2 [35–37]. Combined with the C 1s spectrum in Fig. 4(b, e, h, k), the carbon peak of Li<sub>2</sub>CO<sub>3</sub> at 289.8 eV in the material shows the lowest value than C-S, C-Mg and F-Mg samples, suggesting that the amounts of Li<sub>2</sub>CO<sub>3</sub> on the surface of S-Mg material are less than other materials [10]. This is mainly attributed to the following reasons: on the one hand, more Li<sub>1+x</sub>Ni<sub>0.6</sub>Co<sub>0.2</sub>Mn<sub>0.2</sub>Mg<sub>x</sub>O<sub>2+δ</sub> or Li<sub>x</sub>MgO<sub>2+σ</sub> compounds can possibly form on the surface of materials during synthesis, thereby reducing the formation of Li<sub>2</sub>CO<sub>3</sub>/LiOH [38]. On the other hand, the shell doped Mg is not only effectively enhancing the metal bond energy and maintaining stability of material surface on fresh particles, but also makes it more resistant to H<sub>2</sub>O/CO<sub>2</sub> [39]. In addition, compared with C-S, C-Mg and F-Mg samples, the content of Mg is the highest on the surface of S-Mg material as shown in Fig. 4(a, d, g, j). The above results show that doping Mg on the shell of core-shell structure materials can reduce the cationic mixing degree and the formation of Li<sub>2</sub>CO<sub>3</sub> on the surface of materials.

In order to further study the effect of Mg doping on core-shell structure LiNi<sub>0.6</sub>Co<sub>0.2</sub>Mn<sub>0.2</sub>O<sub>2</sub> materials. The amount of transition metal ions in C-S, C-Mg, F-Mg and S-Mg samples dissolved in the electrolyte was also studied and presented in Fig. 5. It can be

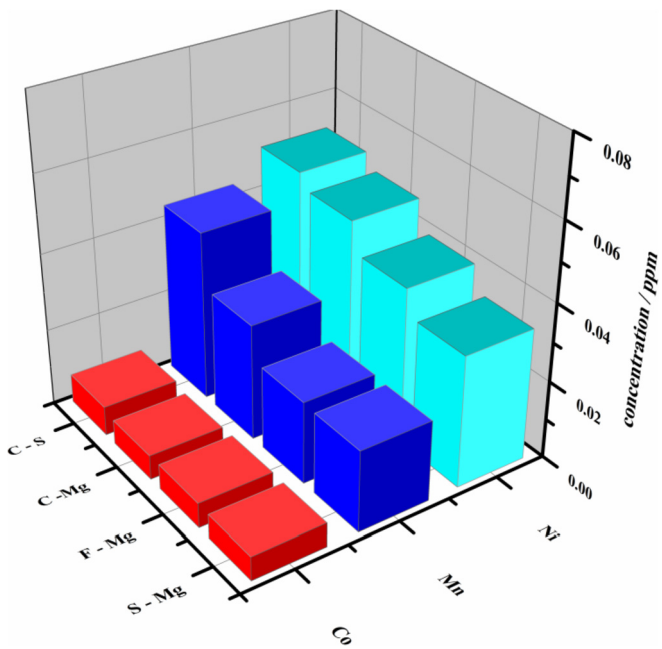


**Fig. 5.** Metal dissolution amount of the C-S, C-Mg, F-Mg and S-Mg samples after storage at 328 K.

observed that the dissolving amount of Ni and Mn in S–Mg samples is much lower than that of C–S, C–Mg and F–Mg samples in the electrolyte for two weeks at 55 °C. In addition, we also observe that the dissolving amount of Co is little in all samples. All the results also show that core-shell structure materials can better inhibit the dissolution of transition metals in materials. Theoretically, the bond dissociation energy of Mg–O ( $\Delta H_f^{298} = 394 \text{ kJ mol}^{-1}$ ) is bigger than that of Ni–O ( $\Delta H_f^{298} = 391 \text{ kJ mol}^{-1}$ ), Mn–O ( $\Delta H_f^{298} = 402 \text{ kJ mol}^{-1}$ ) and Co–O ( $\Delta H_f^{298} = 368 \text{ kJ mol}^{-1}$ ) [22,40]. Thus, doping Mg in the shell effectively enhances the metal bond energy, maintains stability of material surface, and then reduces the dissolution of transition metals in the material [41–44].

### 3.1. Electrochemical results and discussion

The electrochemical performance of C–S, C–Mg, F–Mg and S–Mg sample was evaluated in CR2032 coin type half-cell, in which the potential range from 3 to 4.3 V at a rate of 0.1 C and 0.2 C. As shown in Fig. 6, all materials display similar and smooth curves, indicating that the different Mg doping methods have small changes during charge and discharge. As shown in Table 3, the S–Mg sample exhibits the highest initial discharge specific capacity and coulombic efficiency. In contrast, the C–S sample exhibits the lowest discharge specific capacity and coulombic efficiency. The above results indicate that the discharge capacity and columbic efficiency of core-shell materials can be enhanced by doping Mg on the surface of the shell. Generally, the side reaction between organic electrolyte and electrode will form the CEI, which cause the irreversible capacity in the first cycle. This higher discharge specific capacity and columbic efficiency may be attributed to the fact that the S–Mg simple surface forms a more stable CEI film, thereby reducing the amount of irreversible lithium ions in the materials [45–47].

The cycling performances and coulombic efficiency of the C–S, C–Mg, F–Mg and S–Mg samples at 25 °C under 0.2 C are shown in Fig. 7. The S–Mg sample exhibits a small discharge capacity drop from 183 mAh g<sup>-1</sup> to 157 mAh g<sup>-1</sup> after 100 cycles, with capacity retention of 85.79%. On the contrary, the capacity retentions of C–S, C–Mg, and F–Mg sample after 100 cycles are 69.14%, 72.53%, and 78.93%, respectively. In order to better observe the discharge curve of materials under different cycle times, the discharge curves of the C–S, C–Mg, F–Mg and S–Mg samples at different cycle times are shown in Fig. 8. As detailed description of different cycle times in Fig. 8, with the increase of cycle times, the voltage drop of S–Mg samples is weaker than that of C–S, C–Mg, and F–Mg samples during the process of discharging, implying smaller polarization [48,49]. What's more, the S–Mg sample shows the highest discharge specific capacity and voltage platform after 100 cycles,

which is consistent with the results of Fig. 7. These improvements are partly ascribed to the decrease of the Li<sup>+</sup>/Ni<sup>2+</sup> mixing degree by Mg-doping in shell, which is not only facilitates charge transfer reaction in the layered structure materials [50–52], but also inhibits the transition of material surface from the layered structure to the spinel phase and the salt rock phase [53,54]. On the other hand, owing to the stronger Mg–O bonding, the surface layer doping Mg reduces the side reaction between surface residual alkali and electrolyte during the cycle, further inhibits corrosion of materials by HF in the electrolyte and improves the structural stability [10].

The rate capabilities of C–S, C–Mg, F–Mg and S–Mg samples are displayed in Fig. 9. The discharge capacities of all the cells decrease. However, the S–Mg samples show better rate performance than C–S, C–Mg, and F–Mg. As shown in Fig. 9, the discharge capacity of the S–Mg sample is 128.4 mAh g<sup>-1</sup> at 5 C, which is higher than 108.5 mAh g<sup>-1</sup>, 112.5 mAh g<sup>-1</sup>, 122 mAh g<sup>-1</sup> of the C–S, C–Mg, and F–Mg samples, respectively. Moreover, the capacity of S–Mg cathode can be recovered quickly when discharged at 0.1 C again, further verifying its excellent cycle stability. The significant enhanced rate capability of S–Mg cathode materials may be attributed to the fact that the surface of Mg doping better expands the pathway of Li<sup>+</sup> transfer and effectively enhances the Li<sup>+</sup> conductivity and electron transport in materials [55,56].

The interfacial electrochemistry properties of C–S, C–Mg, F–Mg and S–Mg samples have been investigated by CV curves between 3.0 and 4.3 V at a scan rate of 0.1 mV s<sup>-1</sup> (Fig. 10). The redox reaction gap ( $\Delta V$ ) between the anodic peak and the cathodic peak is considered to show the electrochemical reversibility of electrodes [57]. The  $\Delta V$  values of C–S, C–Mg, F–Mg and S–Mg are 0.292, 0.285, 0.242, and 0.111 V respectively. The  $\Delta V$  values of the S–Mg samples are smallest after first cycle, indicating no obvious polarization and the good cyclic stability during the cycling. This lower polarization may be attributed to the fact that the shell doped Mg can reduce the amount of irreversible lithium ions in the materials and enhance the interface stability for cathode.

Fig. 11 shows the differential curves (d Q/d V) of the C–S, C–Mg, F–Mg and S–Mg samples at 2, 3, 4, 5 and 6 cycles and a cut off voltage of 3–4.3 V at 0.1 C. The oxidation peaks corroborate that all samples underwent a series of phase transitions during charging. While H2→H3 phase transition, situated in 4.2 V, was irreversible and increased mechanical strain that subsequently deteriorated its recharge ability [58]. In comparison with undoped C–S samples, the intensity of the H2→H3 oxidation peak for those Mg doped cathode materials markedly dropped, suggesting Mg doping can inhibit structural phase transition. In addition, Fig. 11 (d) shows that the shell doping is a more effective method to suppress phase transition in contrast to core doping and full doping. This is mainly

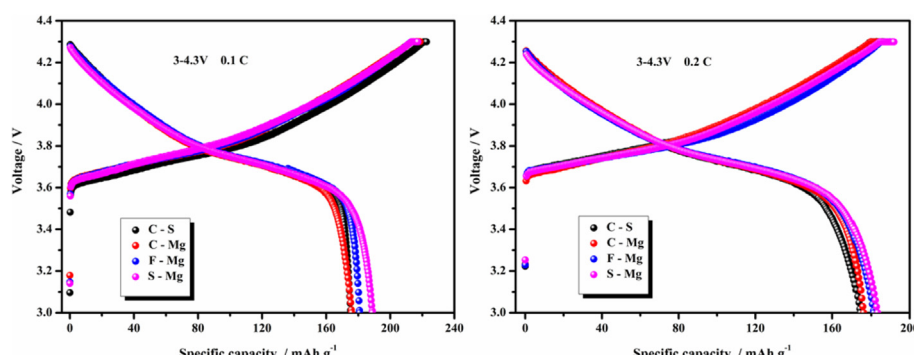


**Fig. 6.** The charge and discharge curves of C–S, C–Mg, F–Mg and S–Mg materials at rate of 0.1 C, 0.2 C between 3 and 4.3 V.

**Table 3**

The discharge specific capacity and coulombic efficiency of C–S, C–Mg, F–Mg and S–Mg samples.

Sample	0.1 C		0.2 C	
	Discharge Specific Capacity (mAh g <sup>-1</sup> )	Coulombic Efficiency (%)	Discharge Specific Capacity (mAh g <sup>-1</sup> )	Coulombic Efficiency (%)
C–S	175.3	78.7%	174.4	93.3%
C–Mg	176.0	80.4%	175.9	94.8%
F–Mg	181.3	83.4%	180.9	95.4%
S–Mg	188.8	86.9%	183.3	95.5%

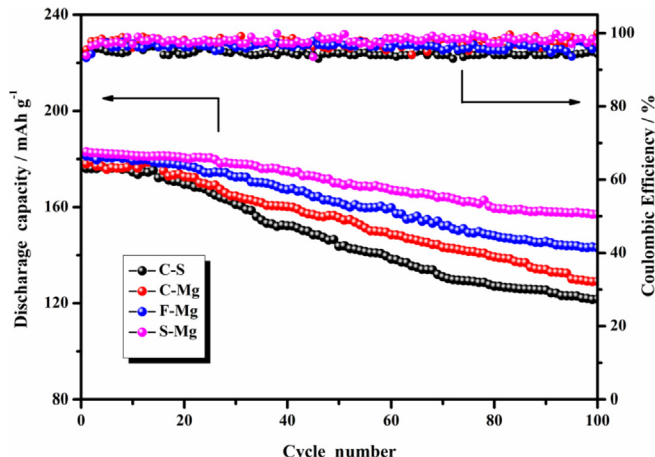


Fig. 7. Cycle performance of the C–S, C–Mg, F–Mg and S–Mg samples at room temperature under 0.2C.

due to the following reasons: On the one hand, the Mg doping in shell layer not only can improve the structural stability of the cathode material, but also reduce the side reactions between the electrolyte and the highly reactive Ni<sup>4+</sup> during the charge and discharge process [59]. On the other hand, the Mg doping in the surface layer can inhibit the formation of H<sub>3</sub> phase in the material, reduce the polarization of the material, and ultimately enhance the cycling and rate performance of the material [36,60].

Electrochemical impedance spectroscopy measurements were carried out to further confirm the improved electrochemical performance of C–S, C–Mg, F–Mg and S–Mg samples. Fig. 12 shows the impedance spectra of C–S, C–Mg, F–Mg and S–Mg electrodes at the charge state of 4.3 V in the 1 st, 50 th and 100 th cycles. All curves are composed of semicircles and a nearly straight line. The semicircle in the high frequency is assigned to the cathode surface R<sub>sei</sub>. The semicircle in medium-to-low frequency is corresponded to R<sub>ct</sub>: charge transfer resistance. Furthermore, the nearly straight line in the low frequency region stands for Warburg resistance. The values of R<sub>sei</sub> and R<sub>ct</sub> are obtained by fitting ZSimpWin software. The corresponding results of R<sub>sei</sub> and R<sub>ct</sub> are shown in Table 4. As can be seen from Fig. 12, with the increase of the number of cycles, the values of R<sub>sei</sub> decrease gradually, while the values of R<sub>ct</sub> increase gradually. This can be interpreted as that there is a self-repair

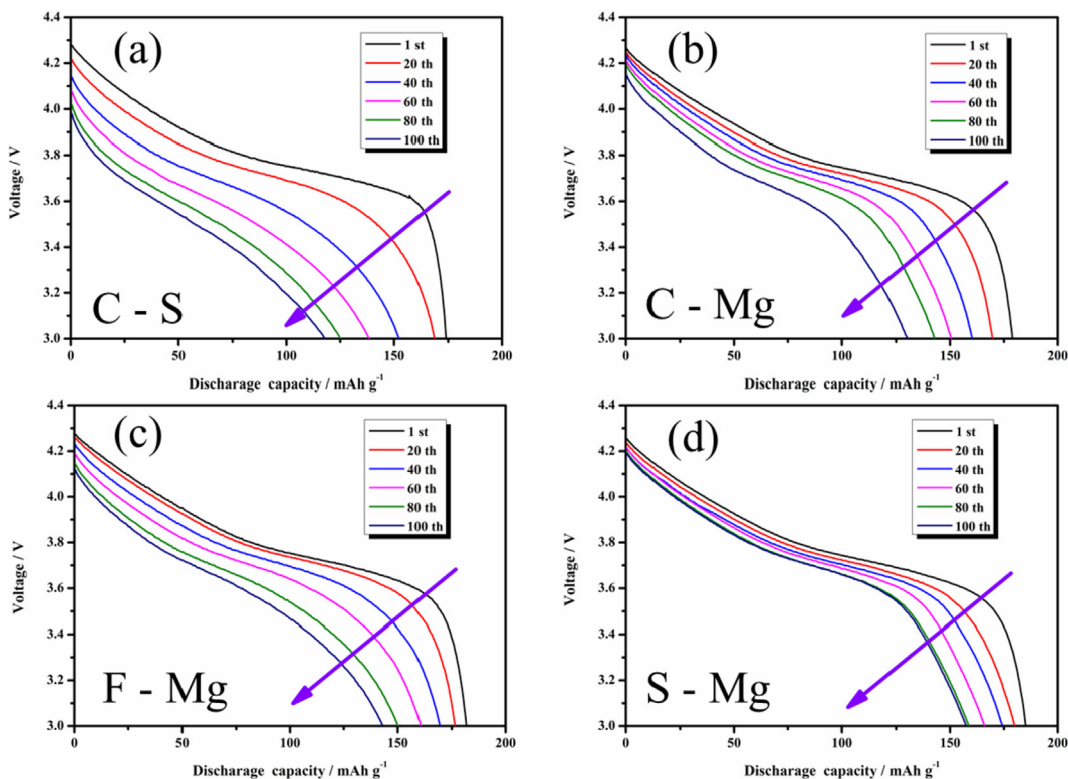
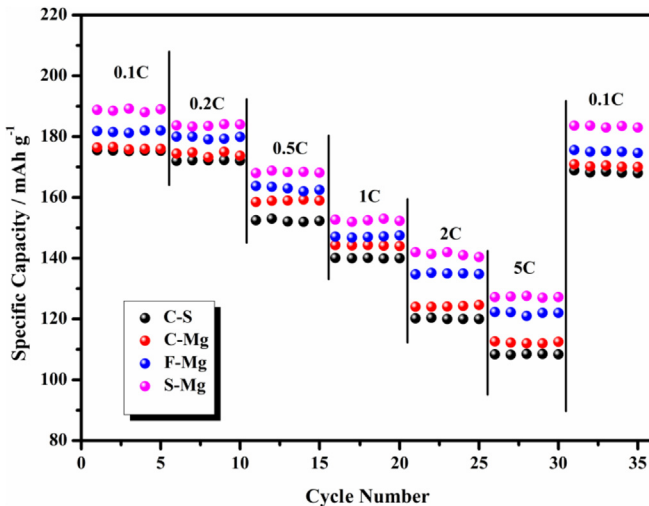


Fig. 8. Discharge curves of the C–S, C–Mg, F–Mg and S–Mg samples at different cycle number.



**Fig. 9.** Rate performance of the C–S, C–Mg, F–Mg and S–Mg samples at different C-rates.

process of CEI in core-shell cathode material. The surface structure degradation compounded by the electrolyte consumption leads to a continuous build-up of an impedance-increasing surface film [61]. Compared with C–S, C–Mg and F–Mg sample, the S–Mg samples shows the lowest  $R_{sei}$  values decreasing from 0.2136 ( $\Omega$  g) to 0.0429 ( $\Omega$  g). This is mainly because Mg doping in shell may inhibit further formation of rock salt on the surface during charge-discharge

process [36]. Meanwhile, the S–Mg sample also shows the lowest  $R_{ct}$  values increasing from 0.0277 ( $\Omega$  g) to 1.6368 ( $\Omega$  g) with the cycle number. Mg doping on the surface can maintain the stability of the material surface and reduce the material impedance [59].

In addition, impedance method was used to estimate the diffusion coefficient of  $\text{Li}^+$  ( $D_{\text{Li}^+}$ ) which was similar in magnitude for the four cathodes in the Table 5 [62,63]. However,  $D_{\text{Li}^+}$  of S–Mg samples was maximum which further certified that the presence of Mg in the shell can enlarge the space in a crystal lattice and facilitate the transfer of  $\text{Li}^+$  during the charging and discharging [64,65]. The results are in agreement with previous results for better rate performance and cycling performance of S–Mg samples.

#### 4. Conclusion

Core-shell cathode material  $\text{Li}[(\text{Ni}_{0.8}\text{Co}_{0.1}\text{Mn}_{0.1})_{2/3}(\text{Ni}_{0.2}\text{C}_{0.4}\text{Mn}_{0.4})_{1/3}]_{2/3}\text{O}_2$  and different Mg doping of core-shell materials (core doping Mg, core-shell co-doped Mg, and shell doping Mg) was successfully synthesized via a co-precipitation method. Compared to core doping Mg and core-shell co-doped Mg materials, the doping Mg in the shell layer materials can enhance the Ni–O bond, reduce the degree of cation mixing, and inhibit the dissolution of transition metals and the formation of  $\text{H}_3$  phase in the material. Furthermore, the doping Mg in the shell layer materials exhibits the optimized electrochemical performance. This excellent electrochemical performance of S–Mg material may be attributed to the Mg doping on the surface not only can maintain the stability of the material surface and reduce the material impedance, but also enlarge the space in a crystal lattice and accelerate lithium ion transport with the presence of Mg in the

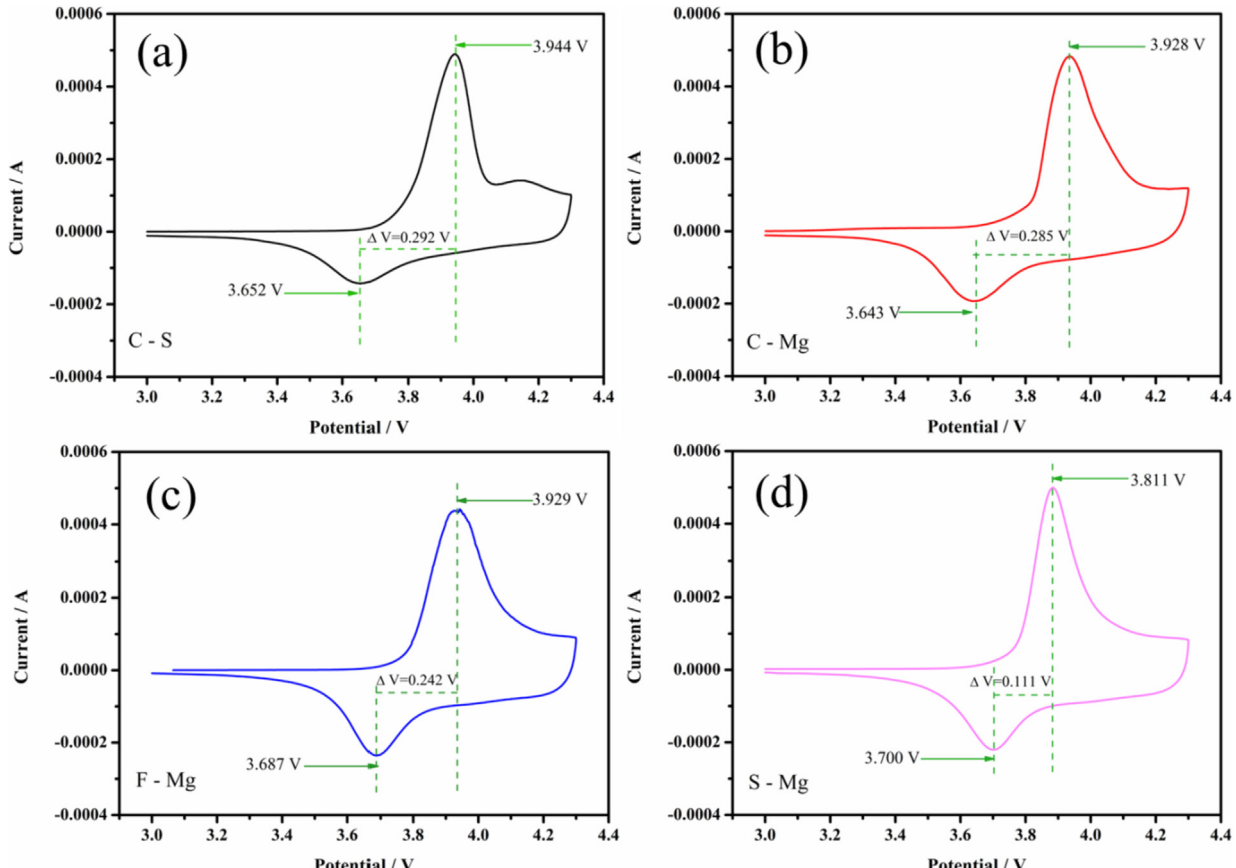


**Fig. 10.** The first cyclic voltammograms of the C–S, C–Mg, F–Mg and S–Mg cell recorded at a scan rate of  $0.1 \text{ mV s}^{-1}$ .

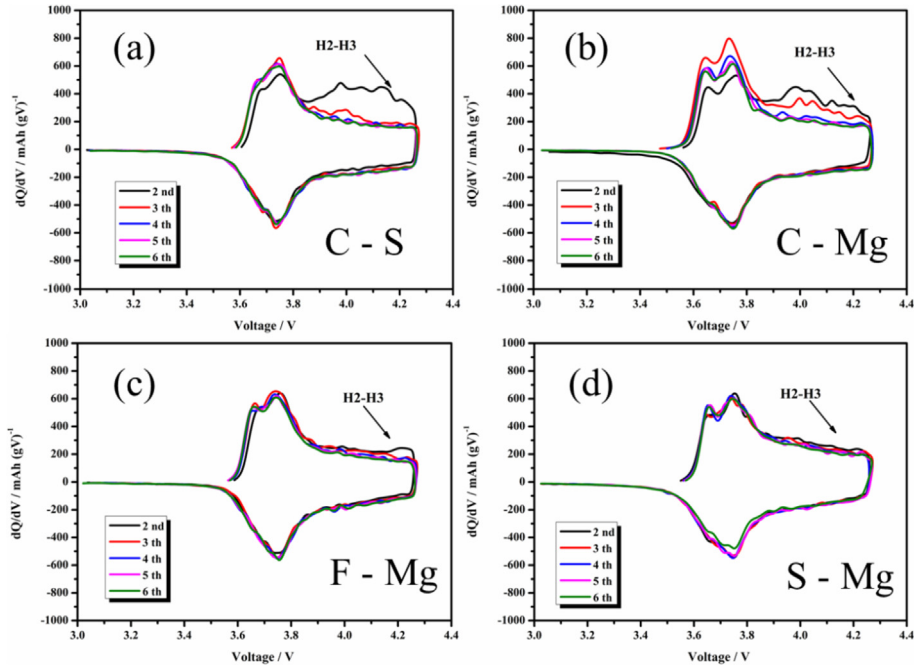


**Fig. 11.** The  $dQ/dV$  curves of the C–S, C–Mg, F–Mg and S–Mg samples at different cycle number.

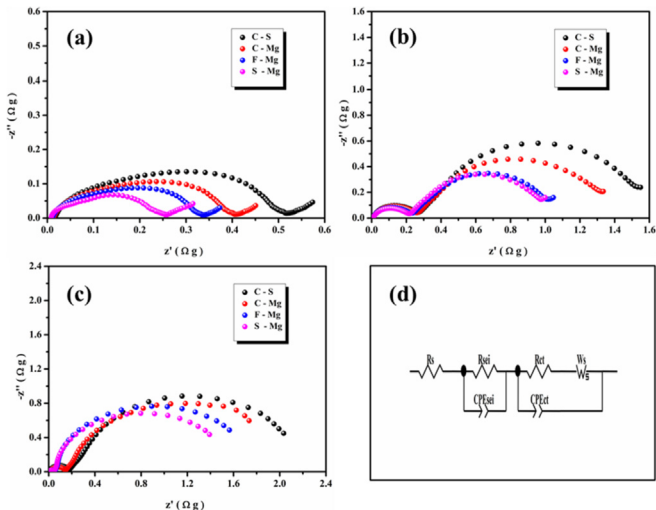


**Fig. 12.** Nyquist plots of C–S, C–Mg, F–Mg and S–Mg (a) 1st, (b) 50th, (c) 100th in the charged state at 4.3 V and equivalent circuit model (d).

**Table 4**  
R<sub>sei</sub> and R<sub>ct</sub> date of the C–S, C–Mg, F–Mg and S–Mg samples.

Sample	R <sub>sei</sub> ( $\Omega \text{g}^{-1}$ )			R <sub>ct</sub> ( $\Omega \text{g}^{-1}$ )		
	1st	50th	100th	1st	50th	100th
C–S	0.3891	0.2617	0.1728	0.1087	1.4020	2.3091
C–Mg	0.3065	0.2562	0.1375	0.0847	1.1109	2.0574
F–Mg	0.2534	0.2272	0.0492	0.0699	0.8081	1.8339
S–Mg	0.2136	0.2113	0.0439	0.0277	0.7316	1.6368

shell during the charging and discharging. Thus, we believe that the doping Mg in the shell layer is deemed to an attractive modification method for enhancing the electrochemical performance of core-shell LiNi<sub>0.6</sub>Co<sub>0.2</sub>Mn<sub>0.2</sub>O<sub>2</sub> materials.

**Table 5**  
DLi + date of the C–S, C–Mg, F–Mg and S–Mg samples.

Sample	DLi+		
	1st	50th	100th
C–S	$2.40 \times 10^{-12}$	$0.28 \times 10^{-12}$	$0.13 \times 10^{-12}$
C–Mg	$2.93 \times 10^{-12}$	$0.37 \times 10^{-12}$	$0.15 \times 10^{-12}$
F–Mg	$3.69 \times 10^{-12}$	$0.78 \times 10^{-12}$	$0.17 \times 10^{-12}$
S–Mg	$4.02 \times 10^{-12}$	$1.15 \times 10^{-12}$	$0.19 \times 10^{-12}$

## Acknowledgements

This work is supported by the Gansu Province Science and Technology Major Project (17ZD2GC011), the High Value Patent Conversion Implementation Project (18ZC1LA014), and the Lanzhou University of Technology Hongliu First-class Discipline Construction Program.

## References

- [1] Y. Wu, T. Cao, R. Wang, F. Meng, J. Zhang, C. Cao, A general strategy of two-dimensional holey cathode nanosheets for superior energy storage, *J. Mater. Chem. A* 18 (2013) 8374–8381.
- [2] Y. Xia, J. Zheng, C. Wang, M. Gu, Designing principle for Ni-rich cathode materials with high energy density for practical applications, *Nano Energy* 49 (2018) 434–452.
- [3] J. Zheng, P. Yan, L. Estevez, C. Wang, J. Zhang, Effect of calcination temperature on the electrochemical properties of nickel-rich LiNi<sub>0.76</sub>Mn<sub>0.14</sub>Co<sub>0.1</sub>O<sub>2</sub> cathodes for lithium-ion batteries, *Nano Energy* 49 (2018) 538–548.
- [4] Q. Wang, C.H. Shen, S.Y. Shen, Y.F. Xu, C.G. Shi, L.H., J.T. Li, S.G. Sun, Origin of structural evolution in capacity degradation for overcharged NMC622 via operando coupled investigation, *ACS Appl. Mater. Interfaces* 29 (2017) 24731–24742.
- [5] J. Zhao, Z. Wang, J. Wang, H. Guo, X. Li, W. Gui, N. Chen, G. Yan, Anchoring K<sup>+</sup> in Li<sup>+</sup> sites of LiNi<sub>0.8</sub>Co<sub>0.15</sub>Al<sub>0.05</sub>O<sub>2</sub> cathode material to suppress its structural degradation during high-voltage cycling, *Energy Technol.* 12 (2018) 2358–2366.
- [6] A. Grenier, H. Liu, K.M. Wiaderek, Z.W. Lebens-Higgins, O.J. Borkiewicz, L. Piper, P.J. Chupas, K.W. Chapman, Reaction heterogeneity in LiNi<sub>0.8</sub>Co<sub>0.15</sub>Al<sub>0.05</sub>O<sub>2</sub> induced by surface layer, *Chem. Mater.* 17 (2017) 7345–7352.
- [7] X. Xiong, Z. Wang, P. Yue, H. Guo, F. Wu, J. Wang, X. Li, Washing effects on electrochemical performance and storage characteristics of LiNi<sub>0.8</sub>Co<sub>0.1</sub>Mn<sub>0.1</sub>O<sub>2</sub>

- as cathode material for lithium-ion batteries, *J. Power Sources* (2013) 318–325.
- [8] S. Bak, E. Hu, Y. Zhou, X. Yu, S.D. Senanayake, S.J. Cho, K.B. Kim, K.Y. Chung, X.Q. Yang, K.W. Nam, Structural changes and thermal stability of charged  $\text{LiNi}_x\text{Mn}_y\text{Co}_z\text{O}_2$  cathode materials studied by combined *in situ* time-resolved XRD and mass spectroscopy, *ACS Appl. Mater. Interfaces* 24 (2014) 22594–22601.
- [9] X. Li, K. Zhang, M. Wang, Y. Liu, M. Qu, W. Zhao, J. Zheng, Dual functions of zirconium modification on improving the electrochemical performance of Ni-rich  $\text{LiNi}_{0.8}\text{Co}_{0.1}\text{Mn}_{0.1}\text{O}_2$ , *Sustainable Energy Fuels* 2 (2017) 413–421.
- [10] T. Chen, X. Li, H. Wang, X. Yan, L. Wang, B. Deng, W. Ge, M. Qu, The effect of gradient boracic polyanion-doping on structure morphology and cycling performance of Ni-rich  $\text{LiNi}_{0.8}\text{Co}_{0.15}\text{Al}_{0.05}\text{O}_2$  cathode material, *J. Power Sources* 392 (2018) 296–296.
- [11] S. Li, X. Fu, J. Zhou, Y. Han, P. Qi, X. Gao, X. Feng, B. Wang, An effective approach to improve the electrochemical performance of  $\text{LiNi}_{0.6}\text{Co}_{0.2}\text{Mn}_{0.2}\text{O}_2$  cathode by an MOF-derived coating, *J. Mater. Chem. A* 16 (2016) 5823–5827.
- [12] X. Xiong, Z. Wang, H. Guo, Q. Zhang, X. Li, Enhanced electrochemical properties of lithium-reactive  $\text{V}_2\text{O}_5$  coated on the  $\text{LiNi}_{0.8}\text{Co}_{0.1}\text{Mn}_{0.1}\text{O}_2$  cathode material for lithium ion batteries at 60 °C, *J. Mater. Chem. A* 4 (2012) 1284–1288.
- [13] P. Hou, X. Wang, D. Wang, D. Song, X. Shi, L. Zhang, J. Guo, J. Zhang, A novel core-concentration gradient-shelled  $\text{LiNi}_{0.5}\text{Co}_{0.2}\text{Mn}_{0.3}\text{O}_2$  as high-performance cathode for lithium-ion batteries, *RSC Adv.* 31 (2014) 15923–15929.
- [14] P. Hou, X. Wang, D. Song, X. Shi, L. Zhang, J. Guo, J. Zhang, Design, synthesis, and performances of double-shelled  $\text{LiNi}_{0.5}\text{Co}_{0.2}\text{Mn}_{0.3}\text{O}_2$  as cathode for long-life and safe Li-ion battery, *J. Power Sources* (2014) 174–181.
- [15] K.S. Lee, S.T. Myung, Y.K. Sun, Synthesis and electrochemical performances of core-shell structured  $\text{Li}[(\text{Ni}_{1/3}\text{Co}_{1/3}\text{Mn}_{1/3})_{0.8}(\text{Ni}_{1/2}\text{Mn}_{1/2})_{0.2}]\text{O}_2$  cathode material for lithium ion batteries, *J. Power Sources* 18 (2010) 6043–6048.
- [16] C. Hua, K. Du, C. Tan, Z. Peng, Y. Cao, G. Hu, Study of full concentration-gradient  $\text{Li}(\text{Ni}_{0.8}\text{Co}_{0.1}\text{Mn}_{0.1})\text{O}_2$  cathode material for lithium ion batteries, *J. Alloy. Comp.* (2014) 264–270.
- [17] E. Lee, H. Noh, C.S. Yoon, Y.K. Sun, Effect of outer layer thickness on full concentration gradient layered cathode material for lithium-ion batteries, *J. Power Sources* (2015) 663–669.
- [18] Z. Sun, D. Wang, Y. Fan, L. Jiao, F. Li, T. Wu, D. Han, L. Niu, Improved performances of  $\text{LiNi}_{0.6}\text{Co}_{0.15}\text{Mn}_{0.25}\text{O}_2$  cathode material with full concentration-gradient for lithium ion batteries, *RSC Adv.* 105 (2016) 103747–103753.
- [19] P. Hou, G. Li, X. Gao, Tailoring atomic distribution in micron-sized and spherical Li-rich layered oxides as cathode materials for advanced lithium-ion batteries, *J. Mater. Chem. A* 20 (2016) 7689–7699.
- [20] U.H. Kim, S.T. Myung, C.S. Yoon, Y.K. Sun, Extending the battery life using an Al-doped  $\text{Li}(\text{Ni}_{0.76}\text{Co}_{0.09}\text{Mn}_{0.15})\text{O}_2$  cathode with concentration gradients for lithium ion batteries, *ACS Energy Lett.* (2017) 1848–1854.
- [21] R. Yu, G. Wang, X. Wang, Di Wang, W. Wen, H. Shu, X. Yang, Design and preparation of a lithium-rich layered oxide cathode with a Mg-Concentration-Gradient shell for improved rate capability, *ChemElectroChem* 9 (2015) 1346–1354.
- [22] Z. Huang, Z. Wang, H. Guo, X. Li, Influence of  $\text{Mg}^{2+}$  doping on the structure and electrochemical performances of layered  $\text{LiNi}_{0.6}\text{Co}_{0.2-x}\text{Mn}_{0.2}\text{Mg}_x\text{O}_2$  cathode materials, *J. Alloy. Comp.* (2016) 479–485.
- [23] K. Tatsumi, Y. Sasano, S. Muto, T. Yoshida, T. Sasaki, K. Horibuchi, Y. Takeuchi, Y. Ukyo, Local atomic and electronic structures around Mg and Al dopants in  $\text{LiNiO}_2$  electrodes studied by XANES and ELNES and first-principles calculations, *Phys. Rev. B* 80 (2008).
- [24] P. Wang, G. Zhang, Z. Li, W.J. Sheng, Y.C. Zhang, J.J. Gu, X.S. Zheng, F.F. Gao, Improved electrochemical performance of  $\text{LiFePO}_4@\text{N}$ -doped carbon nanocomposites using polybenzoxazine as nitrogen and carbon sources, *ACS Appl. Mater. Interfaces* 40 (2016) 15015–15021.
- [25] T. Lei, Y. Li, Q. Su, G. Cao, W. Li, Y. Chen, L. Xue, S. Deng, High-voltage electrochemical performance of  $\text{LiNi}_{0.5}\text{Co}_{0.2}\text{Mn}_{0.3}\text{O}_2$  cathode materials via Al concentration gradient modification, *Ceram. Int.* (2018) 8809–8817.
- [26] Z. Huang, Z. Wang, X. Zheng, et al., Structural and electrochemical properties of Mg-doped nickel based cathode materials  $\text{LiNi}_{0.6}\text{Co}_{0.2}\text{Mn}_{0.2-x}\text{Mg}_x\text{O}_2$  for lithium ion batteries[J], *RSC Adv.* (2015) 88773–88779.
- [27] Z. Huang, Z. Wang, X. Zheng, H. Guo, X. Li, Q. Jing, Z. Yang, Effect of Mg doping on the structural and electrochemical performance of  $\text{LiNi}_{0.6}\text{Co}_{0.2}\text{Mn}_{0.2}\text{O}_2$  cathode materials, *Electrochim. Acta* (2015) 795–802.
- [28] X. Zhao, G. Liang, H. Liu, Y. Liu, Improved conductivity and electrochemical properties of  $\text{LiNi}_{0.5}\text{Co}_{0.2}\text{Mn}_{0.3}\text{O}_2$  materials via yttrium doping, *RSC Adv.* 8 (2018) 4142–4152.
- [29] Y. Xu, W. Xiang, Z. Wu, C. Xu, Y. Li, X. Guo, G. Lv, X. Peng, B. Zhong, Improving cycling performance and rate capability of Ni-rich  $\text{LiNi}_{0.8}\text{Co}_{0.1}\text{Mn}_{0.1}\text{O}_2$  cathode materials by  $\text{Li}_4\text{Ti}_5\text{O}_12$  coating, *Electrochim. Acta* (2018) 358–365.
- [30] Q. Li, R. Dang, Y. Lee, Z. Hu, X. Xiao, A synthesis method for long cycle life lithium-ion cathode material: nickel-rich core–shell  $\text{LiNi}_{0.8}\text{Co}_{0.1}\text{Mn}_{0.1}\text{O}_2$ , *ACS Appl. Mater. Interfaces* 21 (2018) 17850–17860.
- [31] Y. Sun, Z. Chen, H. Noh, D. Lee, H. Jung, Y. Ren, S. Wang, C. Yoon, S. Myung, K. Amine, Nanostructured high-energy cathode materials for advanced lithium batteries, *Nat. Mater.* 11 (2012) 942–947.
- [32] D.W. Jun, C.S. Yoon, U. Kim, Y. Sun, High-energy density core–shell structured  $\text{Li}(\text{Ni}_{0.95}\text{Co}_{0.025}\text{Mn}_{0.025})\text{O}_2$  cathode for lithium-ion batteries, *Chem. Mater.* (2017) 5048–5052.
- [33] D. Song, P. Hou, X. Wang, X. Shi, L. Zhang, Understanding the origin of enhanced performances in core–shell and concentration-gradient layered oxide cathode materials, *ACS Appl. Mater. Interfaces* 23 (2015) 12864–12872.
- [34] Q. Zhang, Y. Su, L. Chen, Y. Lu, L. Bao, T. He, J. Wang, R. Chen, J. Tan, F. Wu, Pre-oxidizing the precursors of Nickel-rich cathode materials to regulate their  $\text{Li}^{+}/\text{Ni}^{2+}$  cation ordering towards cyclability improvements, *J. Power Sources* (2018) 734–741.
- [35] J. Zheng, Z. Yang, Z. He, H. Tong, W. Yu, J. Zhang, In situ formed  $\text{LiNi}_{0.8}\text{Co}_{0.15}\text{Al}_{0.05}\text{O}_2@\text{Li}_2\text{SiO}_4$  composite cathode material with high rate capability and long cycling stability for lithium-ion batteries, *Nano Energy* (2018) 613–621.
- [36] Y. Su, Y. Yang, L. Chen, Y. Lu, L. Bao, G. Chen, Z. Yang, Q. Zhang, J. Wang, R. Chen, S. Chen, F. Wu, Improving the cycling stability of Ni-rich cathode materials by fabricating surface rock salt phase, *Electrochim. Acta* (2018) 217–226.
- [37] Z. Peng, G. Yang, F. Li, Z. Zhu, Z. Liu, Improving the cathode properties of Ni-rich  $\text{LiNi}_{0.6}\text{Co}_{0.2}\text{Mn}_{0.2}\text{O}_2$  at high voltages under 5 C by  $\text{Li}_2\text{SiO}_3$  coating and  $\text{Si}^{4+}$  doping, *J. Alloy. Comp.* (2018) 827–834.
- [38] Y. Chen, Y. Li, S. Tang, T. Lei, S. Deng, L. Xue, G. Cao, J. Zhu, Enhanced electrochemical properties of the Cd-modified  $\text{LiNi}_{0.6}\text{Co}_{0.2}\text{Mn}_{0.2}\text{O}_2$  cathode materials at high cut-off voltage, *J. Power Sources* (2018) 403–413.
- [39] K. Min, S. Seo, B. Choi, K. Park, E. Cho, Computational screening for design of optimal coating materials to suppress gas evolution in Li-ion battery cathodes, *ACS Appl. Mater. Interfaces* 9 (2017) 17822–17834.
- [40] Y. Jiang, Y. Bi, M. Liu, Z. Peng, L. Huai, P. Dong, J. Duan, Z. Chen, X. Li, D. Wang, Y. Zhang, Improved stability of Ni-rich cathode by the substitutive cations with stronger bonds, *Electrochim. Acta* (2018) 41–48.
- [41] J. Kim, H. Ma, H. Cha, H. Lee, J. Sung, M. Seo, P. Oh, M. Park, J. Cho, A highly stabilized nickel-rich cathode material by nanoscale epitaxy control for high-energy lithium-ion batteries, *Energy Environ. Sci.* 6 (2018) 1449–1459.
- [42] H. Zheng, Q. Sun, G. Liu, V.S. Battaglia, Correlation between dissolution behavior and electrochemical cycling performance for  $\text{LiNi}_{1/3}\text{Co}_{1/3}\text{Mn}_{1/3}\text{O}_2$ -based cells, *J. Power Sources* (2012) 134–140.
- [43] W. Li, A. Dolocan, P. Oh, H. Celio, S. Park, J. Chao, A. Manthiram, Dynamic behaviour of interphases and its implication on high-energy-density cathode materials in lithium-ion batteries, *Nat. Commun.* 8 (2017), 14589.
- [44] W. Li, U. Kim, A. Dolocan, Y. Sun, A. Manthiram, Formation and inhibition of metallic lithium microstructures in lithium batteries driven by chemical crossover, *ACS Nano* 6 (2017) 5853–5863.
- [45] X. Chen, F. Ma, Y. Li, J. Liang, B. Matthews, J. Sokolowsk, J. Hana, G. Wu, X. Lu, Q. Li, Nitrogen-doped carbon coated  $\text{LiNi}_{0.6}\text{Co}_{0.2}\text{Mn}_{0.2}\text{O}_2$  cathode with enhanced electrochemical performance for Li-ion batteries, *Electrochim. Acta* (2018) 526–533.
- [46] W. Liu, X. Li, D. Xiong, Y. Haoa, J. Li, H. Kou, B. Yan, D. Li, S. Lu, A. Koo, K. Adair, X. Sun, Significantly improving cycling performance of cathodes in lithium ion batteries: the effect of  $\text{Al}_2\text{O}_3$  and  $\text{LiAlO}_2$  coatings on  $\text{LiNi}_{0.6}\text{Co}_{0.2}\text{Mn}_{0.2}\text{O}_2$ , *Nano Energy* (2018) 111–120.
- [47] L. Xu, F. Zhou, H. Zhou, J. Kong, Q. Wang, G. Yan,  $\text{Ti}_3\text{C}_2(\text{OH})_2$  Coated  $\text{Li}(\text{Ni}_{0.6}\text{Co}_{0.2}\text{Mn}_{0.2})\text{O}_2$  Cathode Material with Enhanced Electrochemical Properties for Lithium Ion Battery, *Electrochim. Acta*, 2018.
- [48] G. Hu, M. Zhang, L. Liang, Z. Peng, K. Du, Y. Cao, Mg–Al–B co-substitution  $\text{LiNi}_{0.5}\text{Co}_{0.2}\text{Mn}_{0.3}\text{O}_2$  cathode materials with improved cycling performance for lithium-ion battery under high cutoff voltage, *Electrochim. Acta* (2016) 264–275.
- [49] Y. Zhang, Z. Wang, F. Yua, L. Quea, M. Wang, Y. Xia, Y. Xue, J. Wu, Studies on stability and capacity for long-life cycle performance of  $\text{Li}(\text{Ni}_{0.5}\text{Co}_{0.2}\text{Mn}_{0.3})\text{O}_2$  by Mo modification for lithium-ion battery, *J. Power Sources* (2017) 1–12.
- [50] D. Wang, Z. Wang, X. Li, H. Guo, Y. Xu, Y. Fan, W. Pan, Effect of surface fluorine substitution on high voltage electrochemical performances of layered  $\text{LiNi}_{0.5}\text{Co}_{0.2}\text{Mn}_{0.3}\text{O}_2$  cathode materials, *Appl. Surf. Sci.* (2016) 172–179.
- [51] C. Xu, W. Xiang, Z. Wu, Y. Xu, Y. Li, M. Chen, X. Guo, G. Lv, J. Zhang, B. Zhong, Constructing protective pillar layer by incorporating gradient  $\text{Mn}^{4+}$  to stabilize the surface/interfacial structure of  $\text{LiNi}_{0.815}\text{Co}_{0.15}\text{Al}_{0.035}\text{O}_2$  cathode, *ACS Appl. Mater. Interfaces* 33 (2018) 27821–27830.
- [52] L. Zou, W. Zhao, Z. Liu, H. Jia, J. Zheng, G. Wang, Y. Yang, J. Zhang, C. Wang, Revealing Cycling Rate Dependent Structure Evolution in the Ni-Rich Layered Cathode Materials, *ACS Energy Lett.*, 2018.
- [53] Q. Ran, H. Zhao, Y. Hu, Q. Shen, W. Liu, J. Liu, X. Shu, M. Zhang, S. Liu, M. Tan, H. Li, X. Liu, Enhanced electrochemical performance of dual-conductive layers coated Ni-rich  $\text{LiNi}_{0.6}\text{Co}_{0.2}\text{Mn}_{0.2}\text{O}_2$  cathode for Li-ion batteries at high cut-off voltage *Electrochim. Acta* (2018) 82–93.
- [54] C. Zhang, S. Liu, J. Su, C. Chen, M. Liu, X. Chen, J. Wu, T. Huang, A. Yu, Revealing the role of  $\text{NH}_4\text{VO}_3$  treatment on Ni-rich cathode materials with improved electrochemical performance for rechargeable lithium-ion batteries, *Nanoscale* 10 (2018) 8820–8831.
- [55] S. Liu, Z. Dang, D. Liu, T. Huang, A. Yu, Comparative studies of zirconium doping and coating on  $\text{LiNi}_{0.6}\text{Co}_{0.2}\text{Mn}_{0.2}\text{O}_2$  cathode material at elevated temperatures, *J. Power Sources* (2018) 288–296.
- [56] O. Breuer, A. Chakraborty, J. Liu, T. Kravchuk, L. Burstein, J. Grinblat, Y. Kauffman, A. Gladikh, P. Nayak, M. Tsubery, A. Frenkel, M. Tlalanker, D. Major, B. Markovsky, D. Aurbach, Understanding the role of minor molybdenum doping in  $\text{LiNi}_{0.5}\text{Co}_{0.2}\text{Mn}_{0.3}\text{O}_2$  electrodes: from structural and surface analyses and theoretical modeling to practical electrochemical cells, *ACS Appl. Mater. Interfaces* (2018) 29608–29621.
- [57] C. Chen, T. Tao, W. Qi, H. Zeng, Y. Wu, B. Liang, Y. Yao, S. Lu, Y. Chen, High-performance lithium ion batteries using  $\text{SiO}_2$ -coated  $\text{LiNi}_{0.5}\text{Co}_{0.2}\text{Mn}_{0.3}\text{O}_2$

- microspheres as cathodes, *J. Alloy. Comp.* 709 (2017) 708–716.
- [58] K.J. Park, H.G. Jung, L.Y. Kuo, P. Kaghazchi, C.S. Yoon, Y.K. Sun, Improved cycling stability of  $\text{Li}[\text{Ni}_{0.90}\text{Co}_{0.05}\text{Mn}_{0.05}]\text{O}_2$  through microstructure modification by boron doping for Li-ion batteries, *Adv. Energy Mater.* (2018) 1–9.
- [59] Y. Li, W. Xiang, Z. Wu, C. Xu, Ya Xu, Y. Xiao, Z. Yang, C. Wu, G. Lv, X. Guo, Construction of homogeneously  $\text{Al}^{3+}$  doped Ni rich Ni-Co-Mn cathode with high stable cycling performance and storage stability via scalable continuous precipitation[J], *Electrochim. Acta* (2018) 84–94.
- [60] B. Jang, J. Son, Structural analysis of iron-doped  $\text{LiNi}_{0.85}\text{Co}_{0.10}\text{Al}_{0.05}\text{O}_2$  cathode materials for lithium-ion batteries, *J. Nanosci. Nanotechnol.* 10 (2016) 10649–10653.
- [61] U. Kim, J. Kim, J. Hwang, H. Ryu, C. Yoon, Y. Sun, Compositionally and structurally redesigned high-energy Ni-rich layered cathode for next-generation lithium batteries, *Mater. Today* (2019) 26–36.
- [62] Y. Chen, Y. Li, W. Li, G. Gao, S. Tang, Q. Sun, S. Deng, J. Guo, High-voltage electrochemical performance of  $\text{LiNi}_{0.5}\text{Co}_{0.2}\text{Mn}_{0.3}\text{O}_2$ , cathode material via the synergistic modification of the Zr/Ti elements, *Electrochim. Acta* (2018) 48–59.
- [63] Y. Shi, M. Zhang, C. Fang, Y. Meng, Urea-based hydrothermal synthesis of  $\text{LiNi}_{0.5}\text{Co}_{0.2}\text{Mn}_{0.3}\text{O}_2$  cathode material, *J. Power Sources* (2018) 114–121 (for Li-ion battery).
- [64] Y. Li, W. Zhao, W. Xiang, Z. Wu, Z. Yang, C.U. Xu, Y. Xu, E. Wang, C. Wu, X. Guo, Promoting the electrochemical performance of  $\text{LiNi}_{0.8}\text{Co}_{0.1}\text{Mn}_{0.1}\text{O}_2$  cathode via  $\text{LaAlO}_3$  coating, *J. Alloy. Comp.* (2018) 546–555.
- [65] S. Gao, X. Zhan, Y. Cheng, Structural, electrochemical and Li-ion transport properties of Zr-modified  $\text{LiNi}_{0.8}\text{Co}_{0.1}\text{Mn}_{0.1}\text{O}_2$  positive electrode materials for Li-ion batteries, *J. Power Sources* (2019) 45–52.